2012 American Control Conference
Fairmont Queen Elizabeth, Montréal, Canada
June 27-June 29, 2012

Wing Trajectory Control for Flapping-Wing Microrobots Using Combined Repetitive and Minimum-Variance Adaptive Methods

Pakpong Chirarattananon*, Néstor O. Pérez-Arancibia*, and Robert J. Wood

Abstract— **We discuss the design and implementation of a combined repetitive and minimum-variance adaptive control strategy for generating *a-priori*-specified desired periodic flapping trajectories of a flying microrobot's wings. With this method and using a static force sensing experimental setup, relevant information about the forces produced by the wings' flapping can be gathered. In turn, this information can be used for designing real-time controllers capable of enforcing desired trajectories on microrobotic insects in vertical flight and hovering.**

I. Introduction

In [1] and [2], it was shown that, by performing static experiments and using modern *linear time-invariant* (LTI) system identification techniques, a significant amount of information can be gathered about the dynamics of flapping-wing microrobots that are similar to the one first presented in [3], which empirically demonstrated the feasibility of flying robotic insects. In [4], employing the static experimental methods developed in [1] and [2], a strategy for controlling the altitude of a constrained, one-degree-of-freedom flapping-wing flying microrobot was developed.

The control strategies applied in the static flapping experiments presented in [1], [2] and [4] were derived from the notion of *adaptive feedforward cancellation* (AFC), commonly employed for rejecting families of periodic disturbances (for examples, see [5], [6] and references therein). The main idea introduced in [1], [2] and [4] is that AFC-based schemes can be used for tracking desired periodic actuator outputs by treating these as output disturbances to be rejected. Also in [1] and [2], it was shown that, simultaneously, the same control strategy can be used for rejecting harmonic disturbances affecting the system. This is important, since a substantial amount of information about the lift forces produced by flapping-wing microrobots can be gathered through experiments in which the robot's flapping angles follow desired sinusoidal trajectories.

An alternative to AFC-based schemes is the use of an LTI strategy based on the *internal model principle* (IMP) [7]. Similar to the adaptive cases described in the previous paragraph, it is possible to think of the desired periodic actuator outputs as disturbances to be rejected, but instead of using an adaptive strategy, the tracking of periodic references and rejection of periodic disturbances can be done through the implementation of LTI IMP-based repetitive controllers [8], [9], [10], [11]. This is the approach pursued here, using the methods developed in [12], [13] and [14], which additionally allow one to combine repetitive and minimum-variance adaptive components in order to track periodic references, and reject harmonic and stochastic disturbances, simultaneously. In the cases presented in this paper, the main challenges are experimental in nature, since the controller design has to consider sensing and actuation limitations at the same time. In order to validate the chosen approach, compelling empirical evidence is presented.

The rest of the paper is organized as follows. Section II describes the flapping-wing microrobot used in the experiments and the experimental setup. Also, this section outlines the control objectives and challenges. Section III describes the proposed repetitive and minimum-variance adaptive control strategies. Simulation and experimental results are presented in Sections IV and V, respectively. Finally, conclusions are given in Section VI.

Notation–

- $\mathbb{R}$ and $\mathbb{Z}^+$ denote the sets of real and non-negative integer numbers, respectively.
- The variable t is used to index discrete time, i.e., $t = \{kT_s\}_{k=0}^{\infty}$, with $k \in \mathbb{Z}^+$ and $T_s \in \mathbb{R}$. As usual, T_s is refered as the sampling-and-hold time.
- The variable τ is used to index continuous time. Thus, for a generic continuous-time variable $x(\tau)$, $x(t)$ is the sampled version of $x(\tau)$.
- z^{-1} denotes the delay operator, i.e., for a signal x, $z^{-1}x(k) = x(k-1)$ and conversely $zx(k) = x(k+1)$, where $x(k) = x(t) = x(kT_s)$.
- $|\cdot|$ denotes the standard module of a complex number.

II. Description of the Experiment

A. Microrobot and Experimental Apparatus

The flapping-wing robotic insect used in the experiments is shown in Fig. 1. This was entirely developed and fabricated at the Harvard Microrobotics Laboratory, based upon designs which previously demonstrated the ability to liftoff [3]. The main components include a piezoelectric bending bimorph cantilever actuator [15], a flexure-based transmission, a pair of airfoils, and an airframe which serves as a mechanical ground. The transmission maps the approximately linear motion of the actuator into the flapping motion of the wings. The transmission consists of links and joints with geometries designed to maximize the product of stroke amplitude and first resonant frequency, given known actuator and airfoil properties.

This work was partially supported by the National Science Foundation (award number CCF-0926148) and the Wyss Institute for Biologically Inspired Engineering. Any opinions, findings, and conclusions or recommendations expressed in this material are those of the authors and do not necessarily reflect the views of the National Science Foundation.

The authors are with the School of Engineering and Applied Sciences, Harvard University, Cambridge, MA 02138, USA, and the Wyss institute for Biologically Inspired Engineering, Harvard University, Boston, MA 02115, USA (email: chirarat@fas.harvard.edu; nperez@seas.harvard.edu; rjwood@eecs.harvard.edu).

* P. Chirarattananon and N. O. Pérez-Arancibia contributed equally to this work.

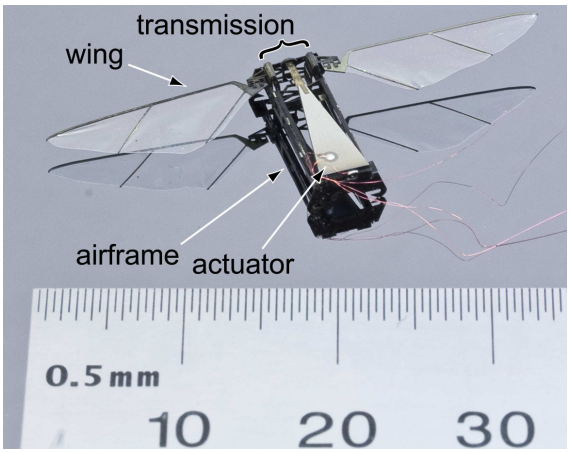

Fig. 1. Photograph of the biologically inspired microrobotic flying insect.

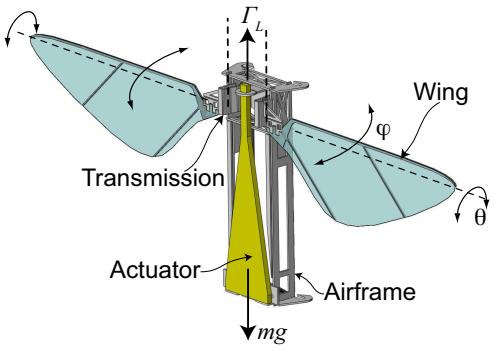

Fig. 2. Illustration of the microrobot employed in the research presented in this article, similar to the one in [3]. This microrobot was entirely designed and fabricated by the authors at the Harvard Microrobotics Laboratory. Γ_L: Average lift force; φ: Flapping angle (also referred as stroke angle); θ: passive rotation angle.

Flight forces are generated through a phenomenon referred to as passive rotation. Here, the wings are connected to the mechanical transmission through flexible hinges, which allow the wings to rotate (angle $\theta(\tau)$ in Fig. 2). This rotation is caused by the inertial forces produced by the flapping $\varphi(\tau)$ and by the aerodynamic forces generated by the interaction of the wings with the air. As explained in [16], an angle θ different than 0° implies that the wings have a positive angle of attack, which causes the generation of lift forces. The microrobot was designed such that, for sinusoidal actuator displacements, drag forces are symmetric about the upstroke and downstroke and the mean lift force vector intersects the center of mass. Thus, ideally, no body torques are generated and the angles of rotation in three dimensions about the robots center of mass (pitch, roll and yaw) should stay at 0°.

In some studies of biological flapping-flight [17], [18], [19], the mean total force, Φ_T, generated by a symmetrical wing pair throughout the stroke is estimated as

$$\Phi_T = \int_0^{\Xi} \rho \overline{C}_\Phi \overline{v_r^2}(\xi) c(\xi) d\xi, \tag{1}$$

which is a standard quasi-steady blade-element formulation of flight force (see [16] and references therein), where ρ is

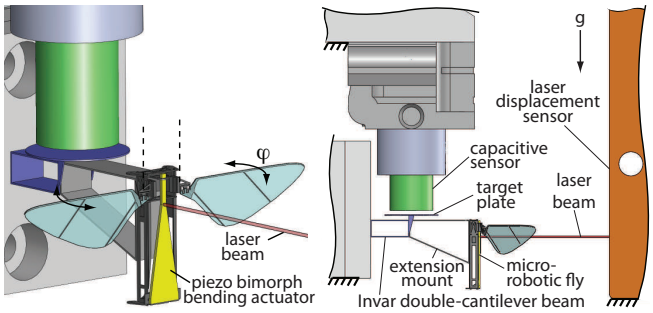

Fig. 3. Setup used in the static flapping experiments. *Left Drawing*: Isometric view. *Right Drawing*: Side view. Here, the flapping microrobot is attached to an Invar double-cantilever beam, whose deflection is measured by a capacitive displacement sensor. This deflection is proportional to the instantaneous lift force generated by the flapping of the wings. The actuator output is measured using a CCD laser displacement sensor.

the density of the air, $\overline{C}_\Phi$ is the mean force coefficient of the wing throughout the stroke, $\overline{v_r^2}(\xi)$ is the mean square relative velocity of each wing section, $c(\xi)$ is the chord length of the wing at a distance ξ from the base, and Ξ is the total wing length. In the case of a sinusoidal stroke of frequency f_r, $\varphi(\tau) = \varphi_0 \sin(2\pi f_r \tau)$, with a horizontal stroke plane, the mean square relative velocity of each wing section can be roughly estimated as

$$\begin{aligned} \overline{v_r^2}(\xi) &= 4\pi^2 f_r^2 \xi^2 \varphi_0^2 \frac{1}{T_r} \int_0^{T_r} \cos^2(2\pi f_r \tau) d\tau \\ &= 2\pi^2 \xi^2 \varphi_0^2 f_r^2, \end{aligned} \tag{2}$$

with $T_r = f_r^{-1}$. This implies that regardless of the size and shape of the wing, the estimated mean total flight force is directly dependent on f_r^2 and φ_0^2. This indicates that in order for flying insects to accelerate against gravity or hover at a desired altitude, they can modulate the average lift force by changing the stroke amplitude, φ_0, or by changing the stroke frequency, f_r. For the robots considered here, the transmission that maps the actuator output, labeled as $y(\tau)$, to the stroke angle $\varphi(\tau)$ can be approximated by a constant κ_T, i.e., $\varphi(\tau) = \kappa_T y(\tau)$. Thus, changing the amplitude and/or the frequency of $y(\tau)$, Φ_T can be modulated.

In steady state, the average discrete-time lift force can estimated as

$$\Gamma_L(t) = \frac{1}{N_L} \sum_{i=0}^{N_L-1} \gamma_L(t - T_s i), \tag{3}$$

where $\gamma_L(t)$ is the sampled version of the continuous-time instantaneous lift force, $\gamma_L(\tau)$. Here, $t = kT_s$, with $T_s \in \mathbb{R}$ fixed and $0 < N_L \in \mathbb{Z}^+$. Note that assuming steady state conditions, for the perfectly symmetric flapping case described in the previous paragraph, $\Gamma_L(t)$ can be thought of as an estimate of Φ_T.

An illustration of the experimental setup employed in the research presented in this paper is shown in Fig. 3. The setup mainly consists of two sensing subsystems: a force sensor and a short range laser position sensor. The first sensor measures instantaneous lift forces by sensing the deflection of a double-cantilever beam to which the microrobot is rigidly connected. The beam deflection is measured using a capacitive displacement sensor. For details on the design

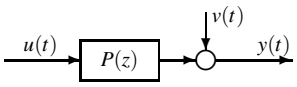

Fig. 4. Idealized system dynamics. $P(z)$: Discrete-time open-loop plant; $y(t)$: Output displacement of actuator; $v(t)$: Output disturbance.

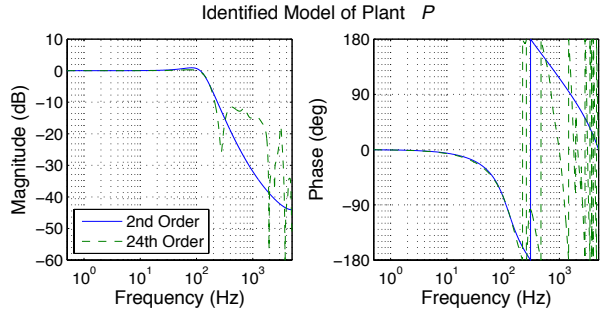

Fig. 5. Bode plot of the identified model $\hat{P}(z)$ of the plant $P(z)$. A 24th-order model is shown in green, a reduced 2nd-order model is shown in blue.

of this force sensor see [20]. The second sensing device in the setup is a CCD laser displacement sensor LK-2001 fabricated by Keyence, used for measuring the piezoelectric actuator displacement output, $y(t)$. These two sensors can be used for estimating two relevant input-output mappings of the flying microrobotic system, which, as described in [4], are essential for designing strategies for altitude control. One is the dynamic mapping from the input voltage to the actuator displacement, labeled as P, whose idealized block diagram is shown in Fig. 4. Here, $u(t)$ is the discrete-time input, $y(t)$ is the measured discrete-time output and $v(t)$ is output disturbance, representing all the disturbances affecting the system, including vibrations generated by the aerodynamic forces produced by the flapping of the wings. The other is the static mapping, labeled as Ψ, from the actuator displacement to the steady-state average lift force, assuming sinusoidal displacements $y(t)$. Thus, $\Psi(A,f)=\Gamma_L$, where A and f are the amplitude and frequency of the displacement $y(t)=A\sin(2\pi ft)$, respectively. Γ_L is the abstract steady-state average lift-force produced by the flapping of the insect's wings, i.e., in (3) $N_L \to \infty$.

As described in the next subsection, an estimate of P can be found using well-known modern system identification methods. On the other hand, in order to estimate Ψ, a controller that forces the output $y(t)$ to follow a desired output signal $y_d(t)=A_d\sin(2\pi f_d t)$ is required. Then, a static mapping or a lookup table relating (A,f) to Γ_L can be computed. In [1], [2] and [4], the controller used for tracking desired outputs with the form $y_d(t)=A_d\sin(2\pi f_d t)$ was designed employing a purely adaptive strategy, based on the AFC scheme. The main contribution of this paper is the introduction of a new approach for solving the problem of estimating Ψ, based on repetitive and minimum-variance adaptive control.

B. Identification of the System Dynamics P

The identification of the system dynamics P is done assuming the LTI structure in Fig. 4. An estimate of P, $\hat{P}$, is found using the *n4sid* algorithm [21], after exciting the system with white noise. The algorithm originally yields a 24th-order state-space discrete-time representation, which is reduced to a 2nd-order model system, using the balanced truncation technique [22], [23]. The resulting models are shown in Fig. 5. Note that for convenience, units are ignored and the identified models have been normalized so that the respective DC gain is 0 dB. The 2nd-order reduced model is used to design a repetitive controller that enforces desired sinusoidal trajectories of the actuator and simultaneously cancels out harmonic disturbances produced by the nonlinear nature of the plant, as described in the next section.

III. Control Strategy

A. Repetitive Control for Reference Tracking

Repetitive control has been proven to be a very effective method for rejecting families of output periodic disturbances, especially when used for canceling the repeatable runout in *hard disk drives* (HDDs) (for example, see [12], [13], [14]). In [1] and [2], it was shown that the dynamic mapping P, when excited in closed loop with a sinusoidal input $u(t)$, can be thought of as an LTI plant affected by an output disturbance $d(t)$ with the form

$$d(t)=r(t)+v(t)=r(t)+h(t)+w(t), \tag{4}$$

where, $r(t)$ is the negative of a sinusoidal reference, i.e., $r(t)=-y_d(t)=-A_d\sin(2\pi f_d t)$ and $v(t)$ is composed of stochastic disturbances, denoted by $w(t)$, and harmonics with frequencies that are integer multiple of f_d, denoted by $h(t)$. Here, through analysis, simulations, and experiments, we show that a repetitive-adaptive strategy can be employed to force the system to follow a desired trajectory and simultaneously cancel output disturbances.

To begin with, without loss of generality, let us for now assume that $w(t)=0$ (i.e., $v(t)=h(t)$), the LTI system P is stable and that $d(t)=r(t)+h(t)$ is *a priori* known. Thus, if, as shown in Fig. 6, a stable feedforward filter K were to be designed so that $d(t)$ is rejected, then

$$z(t)=[Pu](t)+d(t)=[Pu](t)+h(t)+r(t)=0. \tag{5}$$

Note that, consistent with the notation in Section II, the measured actuator output is $y(t)=[Pu](t)+h(t)$ and $r(t)=-y_d(t)$ is generated inside the *digital signal processor* (DSP) used for control. Thus, if (5) is satisfied, it follows that

$$y(t)=-r(t)=y_d(t). \tag{6}$$

In words, the measured actuator output $y(t)$ follows the reference $y_d(t)$. Noticing from Fig. 6 that

$$z=(1-PK)d \tag{7}$$

and recalling the form of $r(t)+h(t)$, the design goal reduces to finding a stable K such that the frequency response of the plant $(1-PK)$ is equal to 0 at frequencies if_d, $0<i\in\mathbb{Z}^+$. This can be done by solving the Diophantine equation

$$RD+KP=1, \tag{8}$$

where R and K are the unknowns and D is an *internal model* with the form

$$D=1-qz^{-N}, \tag{9}$$

in which q is a zero-phase low-pass filter and $N=\frac{f_s}{f_d}\in\mathbb{Z}^+$ (see [14] and references therein). Note that if $\frac{f_s}{f_d}$ is not an

integer, the signal d will be attenuated but not completely annihilated.

As done in [12], [13] and [14], using some of the ideas in [9], [11] and [24], a particular solution pair $\{R_o, K_o\}$ can be found. The method starts by separating P into its minimum and non-minimum phase parts, denoted by P_+ and P_-, as

$$P = P_+ P_-, \tag{10}$$

with

$$P_+(z) = \frac{\beta_+(z)}{\alpha(z)} \quad \text{and} \quad P_-(z) = \beta_-(z), \tag{11}$$

where α, β_+ and β_- are polynomials. All the zeros of β_+ are stable and all the zeros of β_- are unstable. Substituting (11) into (9) we can write

$$RD + \kappa P_- = 1, \quad \text{with} \quad \kappa = KP_+. \tag{12}$$

Among the infinitely many solutions to (12), it is verifiable that one of the solutions is given by

$$\begin{aligned} R_o &= \frac{1}{1-(1-\gamma P_-^* P_-) q z^{-N}}, \\ \kappa_o &= q\gamma P_-^* z^{-N} R_o, \qquad K_o = \kappa_o P_+^{-1}. \end{aligned} \tag{13}$$

Here, P_-^* is defined as $P_-^*(z^{-1}) = P_-(z)$, and $0 < \gamma \in \mathbb{R}$. From this point onwards, in block diagrams and equations we employ the symbols K_o and R_o under the understanding that those correspond to the specific solution in (13).

The block diagram in Fig. 6 assumes that the signal $d = r + h$ is perfectly known. However, in practice h has to be estimated online according the diagram in Fig. 7, where $\hat{d} = \hat{h} + r$ is an estimate of d and $\hat{P}$ is an identified model for the plant P. When the estimation scheme shown in Fig. 7 is employed, the feedforward disturbance cancelation filter K_o becomes part of a feedback controller U_o, connected in the *positive* feedback configuration, computable as

$$U_o = \frac{-K_o}{1 - K_o \hat{P}}. \tag{14}$$

Since U_o is a *single-input-single-output* (SISO) LTI controller, its stability and performance can be analyzed using all the tools of classical control, such as, gain and phase margins, along with the use of sensitivity functions. In this case, we are interested on the output disturbance sensitivity function

$$V_o = \frac{1}{1 - P U_o}. \tag{15}$$

Note that under the assumption $\hat{P} = P$

$$V_o = 1 - P K_o, \tag{16}$$

which is the feedforward mapping from d to y shown in Fig. 6. This implies that the closed-loop performance is not altered by the estimation process, as long as, the model $\hat{P}$ is an exact match of the true plant P. This implies that the closed-loop system in Fig. 7 will be stable for any stable plants P and K_o, under the assumption that $\hat{P} = P$. Thus, nominal stability is guaranteed if the design algorithm produces a stable K_o.

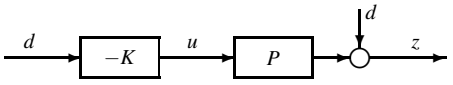

Fig. 6. Feedforward output disturbance rejection scheme used in the design of the repetitive controller K_o, used for tracking references. Here, $d(t) = r(t) + h(t) + w(t)$, where $r(t)$ is the negative of the reference $y_d(t) = A_d \sin(2\pi f_d t)$; $h(t)$ is the sum of all the harmonic disturbances affecting the system; $w(t)$ is the sum of all the stochastic disturbances affecting the system.

Note that K_o is formed by the multiplication of the systems $q\gamma P_-^* z^{-N}$, R_o, and P_+^{-1}. By definition P_+^{-1} is stable. The system $q\gamma P_-^* z^{-N}$ is stable and causal provided that q is stable and that N is large enough. Thus, K_o will be stable as long as R_o is stable. Using the *small gain theorem*, it is possible to show that the stability of R_o is ensured if

$$\left| 1 - \gamma P_-^*(e^{j\theta}) P_-(e^{j\theta}) \right| < \frac{1}{|q(e^{j\theta})|}, \quad \forall \quad \theta \in [0, \pi]. \tag{17}$$

Note that from (17), the real number γ can be regarded as a stability and performance tuning parameter.

B. Repetitive Controller Design

To demonstrate the suitability of the proposed approach, a basic repetitive controller scheme is designed and then modified in order to test some specific ideas pertaining to the control of flapping-wing microrobots. Here, the sample-and-hold rate used by the DSP running the controller is 10 KHz and the desired actuator output y_d is a sinusoid with frequency $f_d = 100$ Hz. Thus, it immediately follows that $N = \frac{f_s}{f_d} = 100$. The other design parameters are $\gamma = 1{,}500$ and

$$q = \left(1 - 10^{-6}\right) \left[2\left(q_0 - q_0^2\right) - \left(2q_0 - q_0^2\right)^2 \right], \tag{18}$$

with

$$\begin{aligned} q_0 &= \left(1 - 10^{-6}\right) \left[2\left(q_1 - q_1^2\right) - \left(2q_1 - q_1^2\right)^2 \right], \\ q_1(z^{-1}, z) &= 0.2z^{-1} + 0.6 + 0.2z. \end{aligned}$$

An estimate of the resulting loop-gain $L = -PU_o$, computed as

$$\hat{L} = -\hat{P} U_o = \frac{P K_o}{1 - K_o \hat{P}}. \tag{19}$$

is shown in Fig. 8. Using this Bode plot and classical control techniques, the robustness of the closed-loop is evaluated. In this case, for $\gamma = 1{,}500$ and the q in (18), the resulting gain and phase margins are 9.85 dB at 4,950 Hz and -96.8° at 4,750 Hz, respectively. This indicates that the closed-loop system is robustly stable and that there is room for playing with the controller gain in order to increase the transient response of the system. Similarly, the performance achieved by the repetitive controller can be evaluated from Fig. 9. There, the first notch at 100 Hz indicates that in steady state the output $y(t)$ will closely follow the reference $y_d(t)$, in the absence of harmonic disturbances. The other notches indicate that when harmonic disturbances are present, these will be rejected by the effect of the controller. Note that once U_o is computed according to the method in the previous subsection, this can be further tuned as

$$U_\delta = \delta U_o, \tag{20}$$

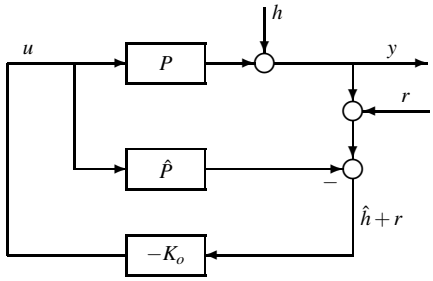

Fig. 7. Estimation of $\hat{h}+r$ and repetitive control scheme. P: True plant; $\hat{P}$: Identified model of P; K_o: Repetitive controller; h: Harmonic output disturbance; $\hat{h}$: Online estimate of h.

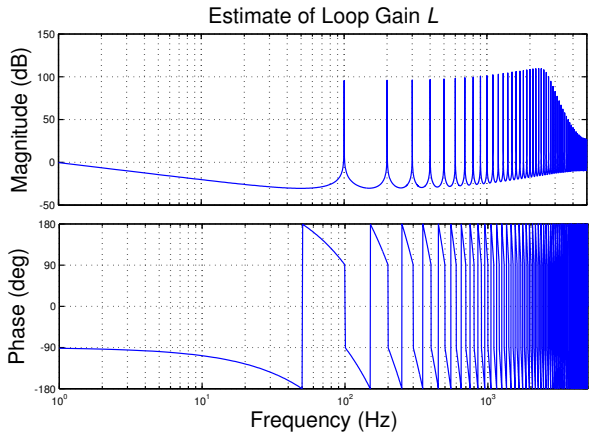

Fig. 8. Estimate of the loop gain L associated with the equivalent controller U_o in (14), connected in the positive feedback configuration. The minimum gain margin is 9.85 dB at 4,950 Hz, and the minimum phase margin is -96.8° at 4,750 Hz.

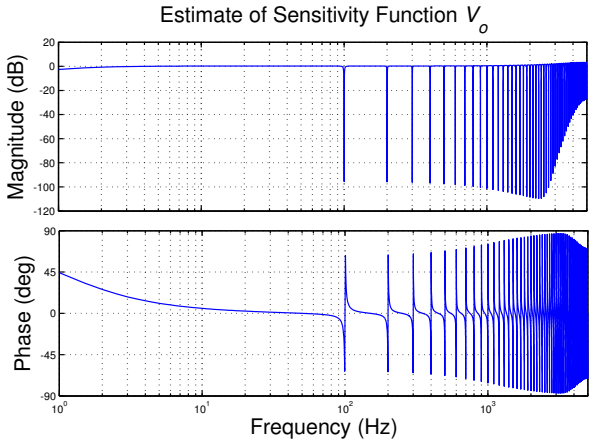

Fig. 9. Estimate of the sensitivity function V_o, calculated from $\hat{P}$ and K_o.

where, $\delta \in \mathbb{R}$ is chosen by evaluating the information in Figs. 8 and 9.

C. Adaptive-Repetitive Control

Thus far we have assumed that the stochastic disturbances are negligible (i.e., $w(t) = 0$). In [12], it was first shown that the solution in (13) is suitable for deriving a scheme that combines repetitive and adaptive elements capable of rejecting periodic and stochastic disturbances simultaneously. Here, we show that the same scheme can be used to track

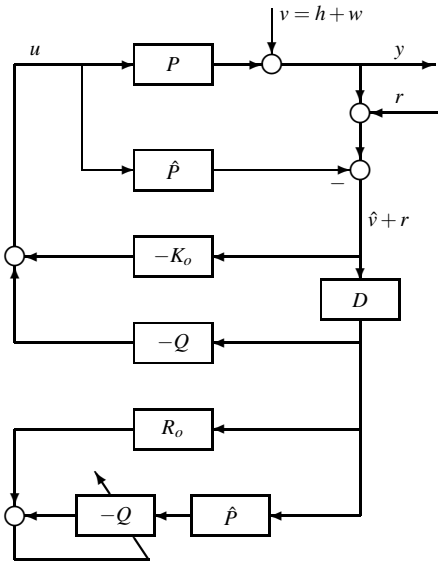

Fig. 10. Block diagram of the adaptive-repetitive control scheme.

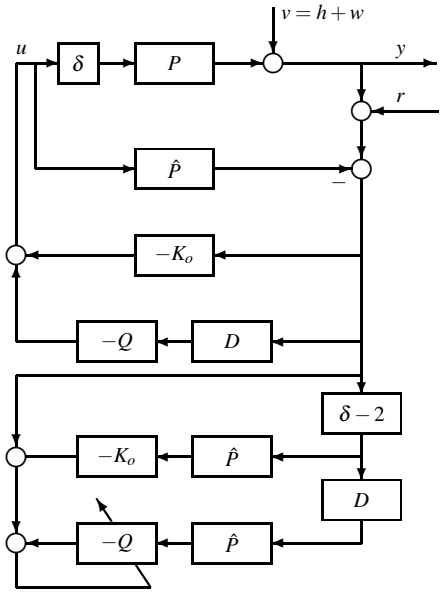

Fig. 11. Block diagram of the adaptive-repetitive control scheme, modified for the use of the tuning parameter δ.

the signal $y_d(t)$, reject the harmonic disturbances $h(t)$ and simultaneously attenuate the stochastic disturbance $w(t)$.

Note that from the pair $\{R_o, K_o\}$, a family of solutions for (8) can be derived as

$$R(Q) = R_o - QG, \qquad K(Q) = K_o + QD, \tag{21}$$

where Q is an arbitrary rational LTI asymptotically stable filter, i.e., $Q \in RH_\infty$. This parametrization allows us to formulate a problem with the objective of minimizing the variance of the system output random variable $\mathbf{z}(t)$, $\forall t$. From this perspective, the sequence $z(t)$ in Fig. 6, and other related figures, can be regarded as a realization of the random process $\mathbf{z}$. Now, let $\mathbf{z}$ be a zero-mean stationary ergodic random process for any given stable LTI filter Q. Then, the

minimum-variance problem can be stated as

$$\min_{Q\in RH_\infty} \mathbf{E}\left\{\mathbf{z}^2(t)\right\}. \tag{22}$$

It is verifiable that (22) is equivalent to the H_2 problem

$$\min_{Q\in RH_\infty} \|\Delta - PK(Q)\Delta\|_2, \tag{23}$$

where Δ is a stable filter that maps a stationary white zero-mean unit-variance random process to the disturbance random process $\mathbf{d}$, whose realization is d in Fig. 6. Filters like Δ are called disturbance models of d. Considering (8) and the parametrized systems $K(Q)$ and $R(Q)$, it follows that (23) is equivalent to

$$\min_{Q\in RH_\infty} \|R_o D\Delta - QPD\Delta\|_2, \tag{24}$$

which can be solved using standard H_2 methods. The solution to (24) requires the disturbance model Δ. In practice, the identification of accurate and reliable disturbance models is extremely difficult and often impossible. Fortunately, (24) can be approximated with the use of adaptive filters, as shown in Fig. 10.

In Fig. 10, the filter Q can be adapted using any adaptive filtering algorithm such as RLS (*recursive least-squares*) or LMS (*least-mean-squares*). Here, the standard LMS and RLS algorithms [25] are employed in both simulations and experiments. In the case shown in Fig. 10, the controller $K(Q) = K_o + QD$ can be broken into a purely repetitive part, K_o, and an adaptive part, QD. Assuming perfect plant matching (i.e., $\hat{P} = P$), the problem being solved recursively is

$$\min_{Q\in RH_\infty} \mathbf{E}\left\{\left[(R_oD - QPD)\,\mathbf{d}(t)\right]^2\right\}, \tag{25}$$

where $\mathbf{d}(t) = r(t) + h(t) + \mathbf{w}(t)$. Note that $\mathbf{w}(t)$ is a random variable, and that, $r(t)$ and $h(t)$ are unknown but deterministic variables. The main idea in the scheme in Fig. 10 is that the adaptive algorithm is run using a regressor constructed using the values from the signal $D(\hat{v}+r)$. Thus, the periodic content in $\hat{v}+r$ is rejected by K_o, and what is left, $D(\hat{v}+r)$, is attenuated adaptively. In the simulations and experiments presented here, we impose the constraint $Q(z) = \sum_{i=0}^{N_Q} \sigma_i z^{-i}$, where N_Q is the order of the filter Q and $\sigma_i \in \mathbb{R}$. This allows us to enforce the stability of Q, since *finite impulse response* (FIR) filters are always stable, provided that the coefficients remain bounded. The convergence properties of the scheme in Fig. 10 can be studied following the approach in [26].

When the tuning parameter δ in (20) is used, the scheme in Fig. 10 no longer minimizes the variance of $\mathbf{z}(t)$, and therefore, a new adaptive structure is required. Here, we proposed the scheme in Fig. 11, in which the signal that is input to the adaptive-repetitive controller is not the estimate of $v+r$, but

$$s = \left[\frac{1}{1+(\delta-1)(K_o+QD)P}\right](\hat{v}+r). \tag{26}$$

This follows from noting that the objective is to adapt a filter Q that minimizes the mean-square of the signal $z = y+r$, which can be expressed in terms of the random variable associated with s, $\mathbf{s}$, as

$$\min_{Q\in RH_\infty} \mathbf{E}\left\{\left[\{1+(\delta-2)K_oP+(\delta-2)QDP\}\,\mathbf{s}(t)\right]^2\right\}. \tag{27}$$

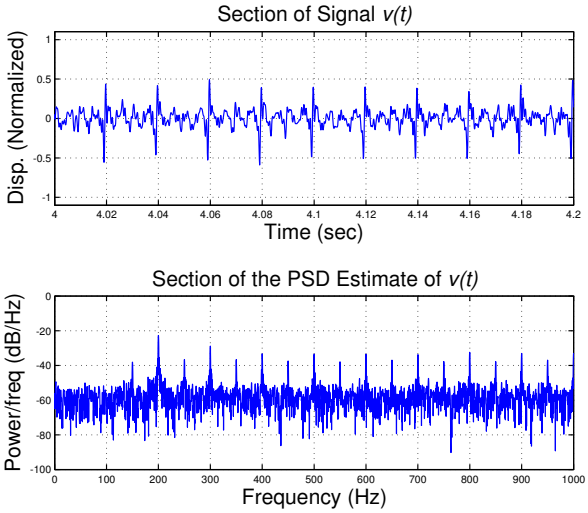

Fig. 12. *Upper Plot:* Section of the time series of the disturbance $v(t) = h(t) + w(t)$, used in the simulations. *Bottom Plot*: PSD of the disturbance $v(t)$, used in the simulations.

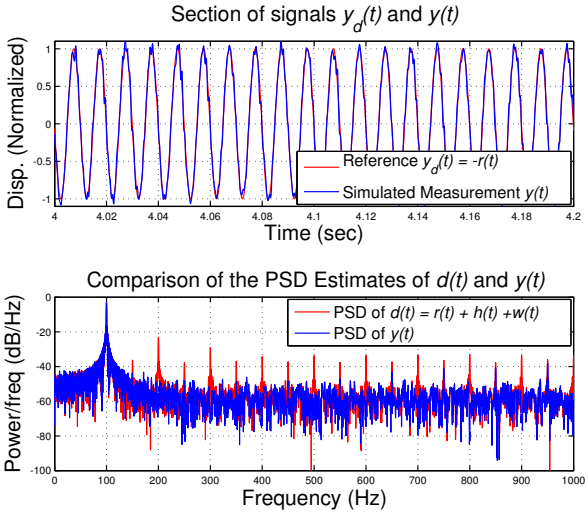

Fig. 13. *Upper Plot:* Section of the time series of the reference $y_d(t)$ and the simulated measurement $y(t)$, obtained using the scheme in Fig. 10 with a 512th-order LMS-based adaptive filter Q. *Bottom Plot*: PSDs of the disturbance signal $d(t) = r(t) + h(t) + w(t)$ and simulated measurement $y(t)$.

When $\delta = 1$, (27) reduces to (25).

IV. Simulations

In this section, we use simulations to exemplify how the methods described in Section III can be employed for signal tracking and for rejecting harmonic and stochastic disturbances simultaneously. Since in simulation the interaction between subsystems and their effect on signals is completely known and repeatable, each component of the control scheme can be understood and explained. The stochastic content in the disturbance $v(t)$, $w(t)$, is generated by filtering white noise through a low-pass filter with a cutoff frequency of 1 KHz (the sample-and-hold rate is 10 KHz). Also, periodic non-harmonic content with frequencies $(if_d + 50)$ Hz, $i \in \mathbb{Z}$, is added to $w(t)$. The harmonic content, $h(t)$, is a sum of sinusoids with frequencies if_d Hz, $i \in \mathbb{Z}$, and accordingly with the design in Section III, $f_d = 100$ Hz. A section of the

TABLE I

SIMULATION RESULTS: EMPIRICAL STANDARD DEVIATION OF THE CONTROL ERROR $z = r + y$, OBTAINED USING THE ADAPTIVE-REPETITIVE (A-R) SCHEME

Algorithm / Order of Q	After 0.3 s		After 4.0 s	
	$\delta = 1.0$	$\delta = 1.5$	$\delta = 1.0$	$\delta = 1.5$
Feedforward	0.1569		0.1148	
Repetitive	0.1235	0.0756	0.0745	0.0758
A-R with LMS / 32	0.1238	0.0761	0.0754	0.0758
A-R with LMS / 64	0.1285	0.0843	0.0768	0.0806
A-R with LMS / 128	0.1295	0.0801	0.0719	0.0771
A-R with LMS / 256	0.1483	0.0921	0.0688	0.0766
A-R with LMS / 512	0.1703	0.0946	0.0670	0.0764
A-R with RLS / 32	0.1264	0.0860	0.0708	0.0688
A-R with RLS / 64	0.1336	0.0945	0.0730	0.0717
A-R with RLS / 128	0.1217	0.0756	0.0676	0.0712
A-R with RLS / 256	0.1238	0.0763	0.0637	0.0662
A-R with RLS / 512	0.1296	0.0904	0.0625	0.0647

disturbance $v(t) = h(t) + w(t)$, in time domain, is shown in the upper plot of Fig. 12. Its corresponding *power spectral density* (PSD) is shown in the bottom plot of Fig. 12.

The effectiveness of the idea proposed in this paper is demonstrated in Fig. 13, which shows the results obtained from using the scheme in Fig. 10 with a 256th-order LMS-based adaptive filter Q (step size $\mu = 0.05$). The upper plot compares the reference $y_d(t)$ with the simulated measurement $y(t)$ and the bottom plot compares the PSDs of $d(t)$ and $y(t)$. The signal y closely follows y_d and the disturbance $v = h + w$ is rejected. The first fact follows from the upper plot in Fig. 13 and from noting that the PSD of y has a spike at 100 Hz. The second fact follows from noting that the harmonic spikes appearing in the PSD of d are annihilated by the control scheme and they do not appear in the PSD of y. In order to highlight the significance of the results in Fig. 13, the feedforward scheme in Fig. 14 is simulated. The corresponding results are shown in Fig. 15. Note that in this case $y(t)$ follows $y_d(t)$ perfectly, however, $v(t) = h(t) + w(t)$ is not attenuated, since as can be seen in the bottom plot of Fig. 15, all the spikes in the PSD of d remain in the PSD of y.

The feedforward case is compared to several closed-loop cases in Table I, where the *empirical standard deviations* (ESDs) of the corresponding control errors $z(t)$ (computed from 300 data points), during the transient (0.3 s) and in steady state (4 s), are shown. Note that the use of a gain $\delta \neq 1$ increases the convergence speed of the algorithms, since for every case the ESD at $Time = 0.3$ is smaller (better) when a gain $\delta \neq 1$ is used. However, there is a noticeable tradeoff, since in every case, the steady-state performance is slightly worse when a gain $\delta \neq 1$ is employed.

V. EXPERIMENTAL RESULTS

The steady-state experimental performances for several cases (with $\delta = 1$) are shown in Table II. In order to obtain these data, a feedforward, a purely repetitive, and several adaptive-repetitive control schemes were implemented. The sample-and-hold rate is 10 KHz, the LMS algorithm was run with a step size $\mu = 0.05$ and the RLS algorithm was implemented with a forgetting factor $\lambda = 0.99999999$ and an initial input variance estimate $\varepsilon = 0.1$. As a benchmark, we choose the feedforward case in which the input to the system

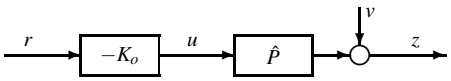

Fig. 14. Block diagram of the feedforward simulation used for analysis and comparison.

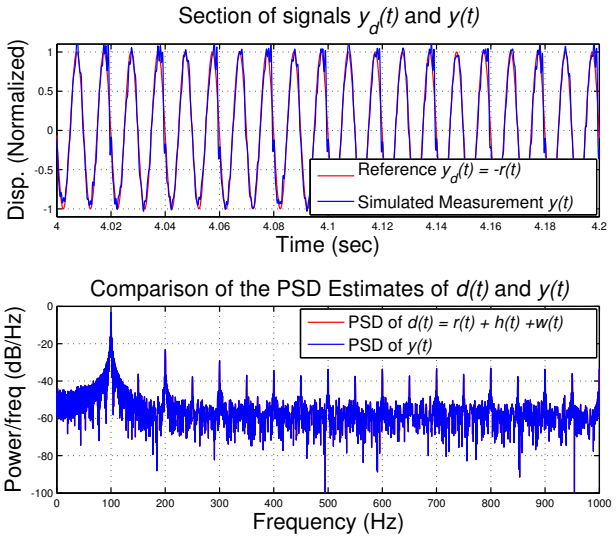

Fig. 15. *Upper Plot:* Section of the time series of the reference $y_d(t)$ and the simulated measurement $y(t)$, obtained using the feedforward scheme in Fig. 14. *Bottom Plot*: PSDs of the disturbance signal $d(t) = r(t) + h(t) + w(t)$ and simulated measurement $y(t)$, obtained using the feedforward scheme in Fig. 14.

P is $u = -K_o r$, as in the simulation in Fig. 14. The time series for the benchmark experimental case is in shown in the upper plot of Fig. 16. Here, the measurement $y_{ff}(t)$ closely follows the reference $y_d(t)$. However, since this scheme is feedforward, no disturbance rejection occurs.

The data in Table II demonstrates that the proposed adaptive-repetitive scheme significantly improves the performance of the system with respect to the feedforward case, with two clear expectable trends: the higher the order of the filter Q, the better the achieved performance; the RLS-based filters perform significantly better than the LMS-based filters with the same order. Note that these two facts are also observed (less dramatically) in simulation (see Table I). The time series of the adaptive-repetitive case, in which an RLS-based adaptive 128th-order filter Q is used, are shown in the middle plot of Fig. 16. Noticeably, the measurement corresponding to this case, $y_{ar}(t)$, follows the reference $y_d(t)$ more closely than $y_{ff}(t)$ does. This is consistent with the data in Table II and with the PSDs in the bottom plot of Fig. 16, which clearly show that the repetitive part of the control scheme eliminates the harmonic spikes from the measurement and that the adaptive part attenuates the stochastic content between harmonic spikes.

VI. CONCLUSION AND FUTURE WORK

Through analysis and experiments, we showed that combined adaptive and repetitive control strategies can be employed for reference tracking and for rejecting harmonic and stochastic disturbances simultaneously in flapping-wing microrobots. This is relevant when the aerodynamics associated with flapping-wing microrobots are experimentally

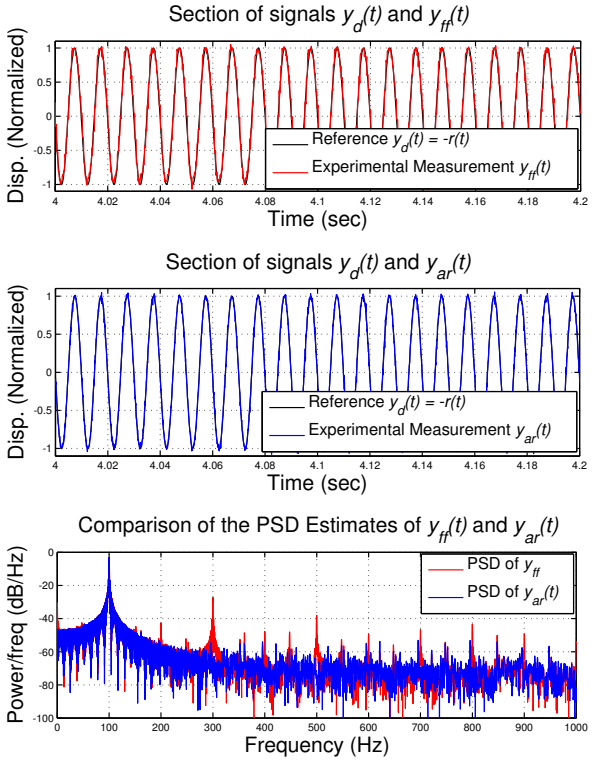

Fig. 16. Experimental example showing the suitability of the adaptive-repetitive scheme in Fig. 10 for tracking a desired trajectory $y_d(t)$ and for rejecting harmonic and stochastic disturbances simultaneously. *Upper Plot*: Benchmark measurement $y_{ff}(t)$, obtained using a purely feedforward scheme ($u = -K_o r$). *Middle Plot*: Measurement $y_{ar}(t)$, obtained using the control scheme in Fig. 10, with a RLS-based Q (128th-order). *Bottom Plot*: Comparison of the PSD estimates of $y_{ff}(t)$ and $y_{ar}(t)$.

TABLE II

EXPERIMENTAL RESULTS: EMPIRICAL STANDARD DEVIATION OF THE CONTROL ERROR $z = r + y$, IN STEADY STATE

Algorithm / Order of Filter Q	After 4.0 s
Feedforward	0.0756
Repetitive	0.0633
Adaptive-Repetitive with LMS / 32	0.0619
Adaptive-Repetitive with LMS / 64	0.0594
Adaptive-Repetitive with LMS / 128	0.0566
Adaptive-Repetitive with LMS / 256	0.0509
Adaptive-Repetitive with LMS / 512	0.0437
Adaptive-Repetitive with RLS / 32	0.0428
Adaptive-Repetitive with RLS / 64	0.0377
Adaptive-Repetitive with RLS / 128	0.0351
Adaptive-Repetitive with RLS / 256	0.0336
Adaptive-Repetitive with RLS / 512	0.0329

studied, since this allows one to enforce desired actuator outputs, which are proportional to the resulting stroke-angle trajectories of the robot. Also, the methods proposed here can be applied in the design and implementation of real-time strategies for altitude control of flapping-wing flying microrobots, provided appropriate sensing systems, which is a matter of future work.

REFERENCES

[1] N. O. Pérez-Arancibia, J. P. Whitney, and R. J. Wood, "Lift Force Control of a Flapping-Wing Microrobot," in *Proc. 2011 Amer. Control Conf.*, San Francisco, CA, Jul. 2011, pp. 4761–4768.

[2] N. O. Pérez-Arancibia, J. P. Whitney, and R. J. Wood, "Lift Force Control of Flapping-Wing Microrobots Using Adaptive Feedforward Schemes," to appear in *IEEE/ASME Trans. Mechatron.*, 2011.

[3] R. J. Wood, "The First Takeoff of a Biologically Inspired At-Scale Robotic Insect," *IEEE Trans. Robot.*, vol. 24, no. 2, pp. 341–347, Apr. 2008.

[4] N. O. Pérez-Arancibia, K. Y. Ma, K. C. Galloway, J. D. Greenberg, and R. J. Wood, "First Controlled Vertical Flight of a Biologically Inspired Microrobot," *Bioinspir. Biomim.*, vol. 6, no. 3, pp. 036 009–1–11, Sep. 2011.

[5] A. Sacks, M. Bodson, and P. Khosla, "Experimental Results of Adaptive Periodic Disturbance Cancellation in a High Performance Magnetic Disk Drive," *ASME J. Dyn. Syst., Meas., Control*, vol. 118, no. 3, pp. 416–424, Sep. 1996.

[6] J. Levin, N. O. Pérez-Arancibia, P. A. Ioannou, and T.-C. Tsao, "A Neural-Networks-Based Adaptive Disturbance Rejection Method and Its Application to the Control of Hard Disk Drives," *IEEE Trans. Magn.*, vol. 45, no. 5, pp. 2140–2150, May 2009.

[7] B. A. Francis and W. M. Wonham, "The internal model principle of control theory," *Automatica*, vol. 12, no. 5, pp. 457–465, Sep. 1976.

[8] T. Inoue, M. Nakano, T. Kubo, S. Matsumoto, and H. Baba, "High Accuracy Control of a Proton Synchrotron Magnet Power Supply," in *Proc. IFAC World Congr.*, Kyoto, Japan, Aug. 1981, pp. 3137–3142.

[9] M. Tomizuka, "Zero Phase Error Tracking Algorithm for Digital Control," *ASME J. Dyn. Syst., Meas., Control*, vol. 111, no. 1, pp. 65–68, Mar. 1987.

[10] S. Hara, Y. Yamamoto, T. Omata, and M. Nakano, "Repetitive Control System: A New Type Servo System for Periodic Exogenous Signals," *IEEE Trans. Autom. Control*, vol. 33, no. 7, pp. 659–668, Jul. 1998.

[11] M. Tomizuka, T.-C. Tsao, and K.-K. Chew, "Analysis and Synthesis of Discrete-Time Repetitive Controllers," *ASME J. Dyn. Syst., Meas., Control*, vol. 111, no. 3, pp. 353–358, Sep. 1989.

[12] N. O. Pérez Arancibia, C.-Y. Lin, T.-C. Tsao, and S. Gibson, "Adaptive–Repetitive Control of a Hard Disk Drive," *in Proc. 46th IEEE Conf. Decision Control*, New Orleans, LA, Dec. 2007, pp. 4519–4524.

[13] N. O. Pérez-Arancibia, T.-C. Tsao, and S. Gibson, "Multiple-Period Adaptive–Repetitive Control of a Hard Disk Drive," *in Proc. Joint 48th IEEE Conf. Decision Control and 28th Chinese Control Conf.*, Shanghai, China, Dec. 2009, pp. 5432–5439.

[14] N. O. Pérez-Arancibia, T.-C. Tsao, and J. S. Gibson, "A new method for synthesizing multiple-period adaptive–repetitive controllers and its application to the control of hard disk drives," *Automatica*, vol. 46, no. 7, pp. 1186–1195, Jul. 2010.

[15] R. J. Wood, E. Steltz, and R. S. Fearing, "Nonlinear Performance Limits for High Energy Density Piezoelectric Bending Actuators," in *Proc. IEEE Int. Conf. Robot. Autom.*, Barcelona, Spain, Apr. 2005, pp. 3633–3640.

[16] J. P. Whitney and R. J. Wood, "Aeromechanics of passive rotation in flapping flight," *J. Fluid Mech.*, vol. 660, pp. 197–220, Oct. 2010.

[17] T. Weis-Fogh, "Quick Estimates of Flight Fitness in Hovering Animals, Including Novel Mechanisms for Lift Production," *J. Exp. Biol.*, vol. 59, no. 1, pp. 169–230, Aug. 1973.

[18] C. P. Ellington, "The Aerodynamics of Hovering Insect Flight. VI. Lift and Power Requirements," *Phil. Trans. R. Soc. Lond. B*, vol. 305, no. 1122, pp. 145–185, Feb. 1984.

[19] F.-O. Lehmann and M. H. Dickinson, "The Control of Wing Kinematics and Flight Forces in Fruit Flies (Drosophila spp.)," *J. Exp. Biol.*, vol. 201, no. 3, pp. 385–401, Feb. 1998.

[20] R. J. Wood, K.-J. Cho, and K. Hoffman, "A novel multi-axis force sensor for microrobotics applications," *Smart Mater. Struct.*, vol. 18, no. 12, pp. 125 002–1–7, Dec. 2009.

[21] P. Van Overschee and B. De Moor, *Subspace Identification for Linear Systems*. Boston, MA: Kluwer, 1996.

[22] A. J. Laub, M. T. Heath, C. C. Paige, and R. C. Ward, "Computation of System Balancing Transformations and Other Applications of Simultaneous Diagonalization Algorithms," *IEEE Trans. Autom. Control*, vol. 32, no. 2, pp. 115–122, Feb. 1987.

[23] G. E. Dullerud and F. Paganini, *A Course in Robust Control Theory*. New York, NY: Springer-Verlag, 2000.

[24] K. J. Åström and B. Wittenmark, *Computer Controlled Systems*. Englewood Cliffs, NJ: Prentice–Hall, 1984.

[25] A. H. Sayed, *Adaptive Filters*. Hoboken, NJ: John Wiley & Sons, 2008.

[26] R. Horowitz, B. Li, and J. W. McCormick, "Wiener-filter-based minimum variance self-tuning regulation," *Automatica*, vol. 34, no. 5, pp. 531–544, May 1998.